ELSEVIER

International Journal of Heat and Fluid Flow 23 (2002) 194–204

International Journal of HEAT AND FLUID FLOW

www.elsevier.com/locate/ijhff

Heat transfer enhancement by Görtler instability

R. Toé [1], A. Ajakh [2], H. Peerhossaini *

Thermofluids and Complex Flows Research Group, Laboratoire de Thermocinétique, CNRS-UMR 6607, Ecole Polytechnique de l'Université de Nantes, Rue Christan Pauc, BP 50609, F-44306, Nantes Cedex 3, France

Abstract

Measurements of mean velocity field and mean temperature field were performed in a concave boundary layer. The growth of the induced Görtler vortices embedded in this boundary layer has been determined in two ways by a criterion based equally on spanwise distortion of velocity or temperature profile. The streamwise and spanwise evolution of heat transfer coefficient has been determined by measurement of wall temperature. It was found that the steady growth of these structures induces a characteristic plateau in the evolution of Stanton number versus Reynolds number. This plateau starts with the enhancement of the amplification criterion and finishes when the transition occurs. © 2002 Elsevier Science Inc. All rights reserved.

1. Introduction

The past fifty years have seen the tremendous development of jet engine propulsion. In this half century of research and development, turbine inlet temperatures have been increased dramatically. "State-of-the-art" turbines operate today at average temperatures exceeding 2000 K. Under such extreme conditions, the prediction of heat transfer becomes one of the main tasks which the turbine designer has to deal with and successfully estimating the heat load on the blading is essential.

This is particularly true on the pressure side of turbine blades where strong curvature effects occur on a surface where the pressure exhibits strong gradients alternatively negative and positive. It has long been recognized that the boundary layer on such typical concave surfaces may present instabilities which result in the appearance of longitudinal vorticies known as Görtler vortices. These vortices have a great impact on the development of the boundary layer and considerably affect heat transfer. Boundary layer codes commonly used in gas turbine design do not explicitly take into account these instabilities and the turbine designer is therefore often exposed to difficulties in assessing the precise heat load on blade pressure sides.

The effect of Görtler vortices is also very important in the film cooling of gas turbine blades. The counter-rotating motion of the Görtler vortices destroys the layer of the cold air injected on the blade surface in order to prevent its burning by the hostile combustion products (Peerhossaini and Wesfreid (1988a)).

Experimental evidence of Görtler vortices is a common feature of many hypersonic flow fields. Their existence seems enhanced by gradients induced by high Mach numbers on concave walls. For re-entry spaceplanes, the main field of interest is related to the local overheating pattern that comes mainly from flaps deflection. The knowledge of over heatings, or peaks over mean values of thermal fluxes, is crucial for such vehicles, due to direct interaction with allowable center of gravity margins of location.

In general, boundary layers with curved streamlines appear in many situations in nature and in technology. They are susceptible to an instability mechanism of centrifugal type often called Görtler instability (Görtler, 1940). The unstable regime consists of a laminar boundary layer over which an array of longitudinal vortices (Görtler vortices) is superposed. When they begin to appear, Görtler vortices are steady. However, when the control parameter (Görtler number $G_\theta = (U_n\theta/v^*)(\theta/R)^{1/2}$, where U_n is the nominal velocity, θ the momentum thickness, v the fluid viscosity and R the radius of curvature) is increased, they undergo a

* Corresponding author. Tel.: +33-2-40-68-31-39; fax: +33-2-40-68-31-41.

E-mail address: hassam.peerhossaini@isitem.univ-nantes.fr (H. Peerhossaini).

[1] Present address: Thermodyn, B.P. 119, 71203 Le Creusot Cedex, France.

[2] Present address: AXA Global Structured Products Inc., 600 Fifth Avenue, New York, NY 10020, USA.

0142-727X/02/$ - see front matter
PII: S0142-727X(01)00149-7

Nomenclature

C_p	heat capacity (J/kg K)
G	Görtler number ($\frac{U_n\theta}{\nu}\sqrt{\theta/R}$)
Gr	Grashof number ($\frac{g\beta\Delta T}{\nu^2}(\frac{\nu x}{U_n})^{-3/2}$)
m	mass (kg)
P_z	perturbation criterion based on $\partial U/\partial z$
P_{zT}	perturbation criterion based on $\partial T/\partial z$
R	wall radius of curvature (m)
Re	Reynolds number ($U_n x/\nu$)
St	Stanton number ($h/\rho C_p$)
T	local temperature (K)
t	time (s)
T_∞	free stream temperature (K)
T_w	wall temperature (K)
U	longitudinal component of velocity (m/s)
U_n	free stream velocity or nominal velocity (m/s)
U_{pw}	potential wall velocity (m/s)
x	streamwise direction (m)
y	normal to the wall direction (m)
z	spanwise direction (m)
β	linear growth rate (m^{-1})
λ	spanwise forced wavelength (m)
μ	dynamic viscosity (N s/m^2)
ν	kinematic viscosity (m^2/s)
ρ	density (kg/m^3)
φ_w	wall heat flux (W/m^2)
θ	momentum thickness (m)

secondary instability and eventual breakdown into turbulence (Peerhossaini and Wesfreid (1988b); Peerhossaini and Wesfreid (1988c)).

Görtler vortices embedded in the boundary layer affect heat, mass, and momentum transfer between the solid wall and the fluid (Peerhossaini, 1997). Therefore, the different dynamical states up to the transition through which the Görtler vortices evolve leave a distinct signature on the wall. Heat transfer has proved to be very sensitive to this evolution.

The effect of Görtler vortices on heat transfer was first addressed by McCormack et al. (1970). Experiments were carried out in a boundary layer with free-stream turbulence intensity less than 1%. The concave wall had a radius of curvature of 13 cm and the Görtler number G_δ varied between 16 and 240. Cold experiments were run and the curved wall was covered with a thin film of methyl alcohol saturated with naphthaline. These experiments showed wall striations with wavelength $\lambda = 0.5$ cm. Heat transfer experiments were carried out in constant wall heat flux conditions and the Nusselt number was computed from surface temperature measurements. The ratio of the curved-wall Nusselt number to the flat-plate Nusselt number increased by 30–190%, with an average of 110% beyond the flat-wall Nusselt number. However, there were too few experimental points to determine whether they follow a waveform and therefore can be related to the Görtler vortex pattern.

A series of experiments on heat-transfer enhancement by Görtler vortices was carried out by Crane and Sabzvari (1989) and Crane and Umur (1990). The water tunnel experiments of Crane and Sabzvari were performed with constant wall heat flux conditions at Reynolds number Re_r (based on the wall radius of curvature) ranging between 8400 and 27,100. The Görtler number beyond which heat transfer enhancement became observable was $G_\theta = 10$. The heat transfer experiments of Crane and Umur were made in a wind tunnel with wall radius concave curvature of 254 cm. Measurements were made for $Re = 8.47 \times 10^5$ and free stream turbulence intensity between 0.2% and 0.5%. The wavelength of Görtler vortices, which was fixed by the final screen of the settling chamber, was 2 cm. With zero axial pressure gradient, the spanwise averaged Stanton number (St) increased rapidly to a turbulent value if the flat-plate pre-curvature boundary layer was allowed to develop so that G_θ at the beginning of the curved wall was 10. Without a pre-curvature boundary layer, G_θ was 5 at the start of curvature and the Stanton number increase was delayed until G_θ reached 10 again. From these experiments it seems that $G_\theta = 10$ is the value beyond which nonlinear effects become dominant and increase heat transfer.

McCormack et al. (1970) gave a linear analysis of the incompressible Navier–Stokes and energy equations using the normal mode solution. An approximate relation of the ratio of Nusselt number for a curved surface (Nu_c) to the flat-plate Nusselt number (Nu_f) for unit Prandtl number was obtained: $Nu_c/Nu_f = 1 + 0.6\cos(\alpha z)$. Thus the linear analysis shows that the ratio of the Nusselt number fluctuates sinusoidally around the spanwise averaged value with an amplitude of 60%. However, the overall enhancement of heat transfer is zero. This result was expected because of the linear nature of the analysis.

Smith and Haj-Hariri (1993) studied the weakly nonlinear regime of the Görtler instability as an intermediate step in the evolution from a linear to a nonlinear state. They found a moderate net increase of span-independent heat transfer from the wall. The fully nonlinear problem was addressed by Liu and Lee (1995). They solved nonlinear Navier–Stokes and energy equations by using the initial shape of disturbances borrowed from the linear solution of Floryan and Saric (1982). The disturbance amplitude was obtained by equating its

maximum spanwise root mean square value to the experimental measurements of Swearingen and Blackwelder (1985). For initial conditions in the energy equation they used also the solution to the linearized scalar transport equation by using the velocity field given by Floryan and Saric (1982). Their results showed a markedly increased Nusselt number over that of Blasius boundary layer, especially in the nonlinear region where it can reach 400% for $Pr = 7.07$.

In this paper we report on a parallel heat transfer and fluid mechanics study of the amplification of perturbations in a curved boundary layer under Görtler instability. In particular, we define a perturbation amplification criterion that allows detection of nonlinear saturation of perturbation growth and the onset of the transition to turbulence in a curved boundary layer. The Stanton number was used to examine the relation between the growth of perturbations and transition with the wall heat transfer. We show that there is a good agreement between these two phenomena.

2. Experimental apparatus

Experiments were carried out on the concave boundary layer of a concave–convex model mounted in a laminar open-loop wind tunnel. Flow is generated by suction using a six-blade fan of 1.18 m diameter and an 11 kW power electric motor. The nominal freestream velocity could vary between 1 and 9 m/s with 2% stability and a constant turbulence intensity of 0.7%. The tunnel is equipped with a 2-m long settling chamber of 1.10 m × 1.20 m cross-section in which two honeycombs and five grids are fixed. The settling chamber is followed by a nozzle of 4.7 area contraction ratio that connects the chamber to the test section. More details on the wind tunnel and concave–convex model used in this work can be found in Peerhossaini and Bahri (1998).

A concave–convex model similar to that of Peerhossaini et al. (1990) was used. The model shown in Fig. 1 has four main parts:

- the leading edge in the shape of a thick laminar airfoil (NACA-0025);
- the concave part (radius of curvature 65 cm) in which the measurements were carried out;
- the convex part (radius of curvature 15 cm);
- the trailing edge, a flat plate that can rotate around the center of curvature of the convex section.

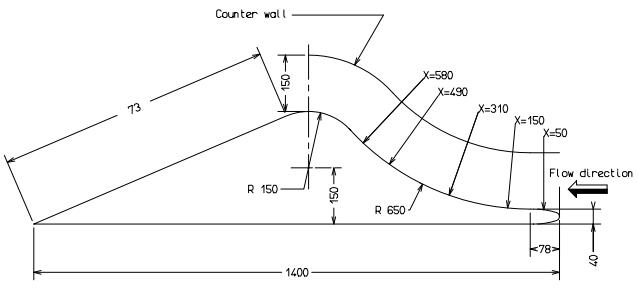

Fig. 1. Schematic diagram of the model.

The origin of the curvilinear axial coordinate x is fixed at the leading edge, and the concave wall starts at $x = 9$ cm. Velocity and temperature fields are measured on the concave wall in the range 10 cm $< x <$ 60 cm. Görtler vortices are generated as the result of amplification by the centrifugal instability of upstream perturbations entering the concave boundary layer. It has been shown that Görtler instability does not have a natural wavelength selection mechanism (like Rayleigh–Bénard or Taylor–Couette instabilities) (Guo and Finlay, 1994); instead, it amplifies the wavelengths imposed by the rig facilities on the incoming flow (Kottke, 1988). Therefore, in this study the spanwise position of the Görtler vortices was fixed by forcing a pre-determined wavelength upstream of the leading edge. This was done by a perturbation grid made of 0.19-mm-diameter wires with 30-mm wavelength placed vertically 4 mm upstream of the leading edge. This wavelength was chosen to reinforce the pseudo-natural wavelength of the incoming flow that was imposed by the last honeycomb of the settling chamber. The effect of perturbation wires on vortex generation has been reported elsewhere (Ajakh et al., 1999). A traversing mechanism in the wind tunnel provided probe movements in the x, y and z direction. The step size of probe movement in the normal to the wall direction was 7 μm.

Mean and fluctuating velocity fields were measured by a hot-wire anemometry system (streamline-Dantec). The analog signal was digitized at 100 Hz through a 16-bit resolution analog–digital converter (Iotech ADC488/8SA). The sampling time was at least 60 s. Special curved hot-wire probes were used that allowed a very close approach to the wall. The diameter of the sensitive part of the hot wire was 5 μm and its length was 3 mm. The prongs of the probe had a 50 μm diameter, so that the probing range was limited to 50 μm from the wall. The nominal flow velocity was measured by a Pitot tube and the three-dimensional positioning of the probe and all data acquisition were carried out by a microcomputer through an IEEE interface.

The model surface was heated with a constant heat flux and was covered with a thin (130 μm) resistance film composed of a 70 μm constantan layer glued onto a 60 μm Kapton film. The resistance film, of dimensions 120 cm × 45 cm × 130 μm, was fixed on the model surface by double-faced adhesive film that resists humidity and can tolerate temperatures as high as 100 °C. The constantan film was heated by the Joule effect using a DC stabilized power supply (SORENSEN DCS 8V-125A). The resistance sheet was connected to the power supply

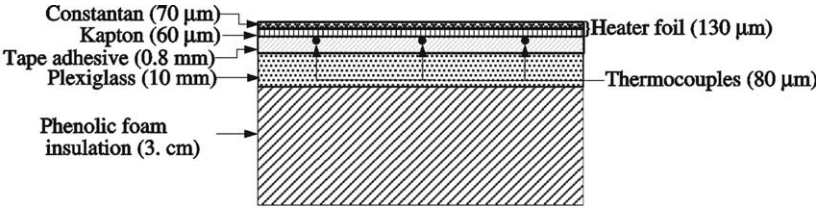

Fig. 2. Instrumentation of the model wall.

through two 45-cm long copper rods of 5 mm × 5 mm cross-section soldered on the whole width of the constantan sheet. The copper rods were then connected to the power supply by six wires of equal electric resistance soldered on equal distances along the rods. These precautions were taken in order to assure a uniform distribution of electric current through the resistance sheet and therefore a uniform wall heat flux. 196 chromel–alumel thermocouples of 80 μm bead measured the temperature on the Kapton side of the heating film. They were embedded between the back of the heating film and the double-faced adhesive film (Fig. 2). Thermocouples were arranged in three lines in the streamwise flow direction. Each line was composed of 40 thermocouples, and the distance between the lines was 1.5 cm. In the longitudinal direction the distance between each neighboring thermocouple was 2 cm for 5 cm $< x <$ 57 cm and 1 cm for 57 cm $< x <$ 70 cm. In order to follow the temperature variations in the upwash and downwash regions, 15 thermocouples were implanted in the spanwise direction at each of the following stations: $x = 5$, 15, 31, 49, and 58 cm. The distance between the thermocouples was not uniform; in the upwash region the distance was smaller, around 5 mm (Fig. 3). Temperature signal acquisition was carried out by a Keithley system composed of an 80-channel scanner (2000 SCAN series) and a multimeter (K199) connected to the microcomputer via an IEEE interface.

In order to reduce heat loss from the back of the model wall, it was insulated with phenolic foam ($\lambda = 0.02$ W/mK) in which eight thermocouples were implanted. Measurements showed that heat losses by conduction from the back side of the model were 6 to 8 W/m^2, that is between 3% and 4% of the imposed flux.

The temperature field in the boundary layer was measured by a thermocouple (K-type) probe. The chromel and alumel wires of the thermocouple were of 12 μm diameter. The probe was similar to the curved hot-wire probe used for the velocity measurements (Blackwell and Moffat, 1975). Temperature signal acquisition was carried out in the same way as for the wall thermocouples.

3. Results

3.1. Effect of wall heating

Wall heating can destabilize the boundary layer by natural convection. If such a phenomenon occurs it can interfere with the destabilizing effects of the Görtler instability and thus make the interpretation of the

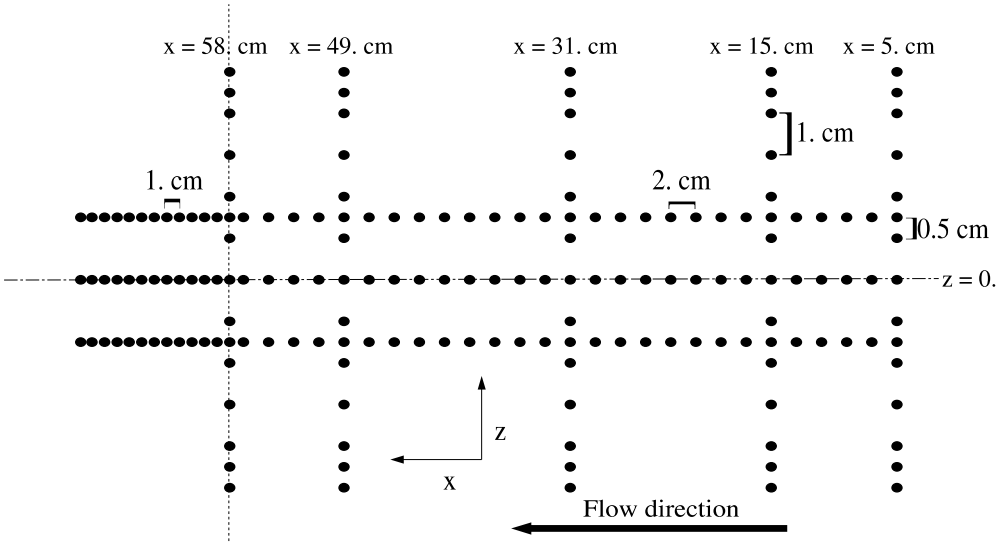

Fig. 3. Position of the embedded thermocouples in the wall.

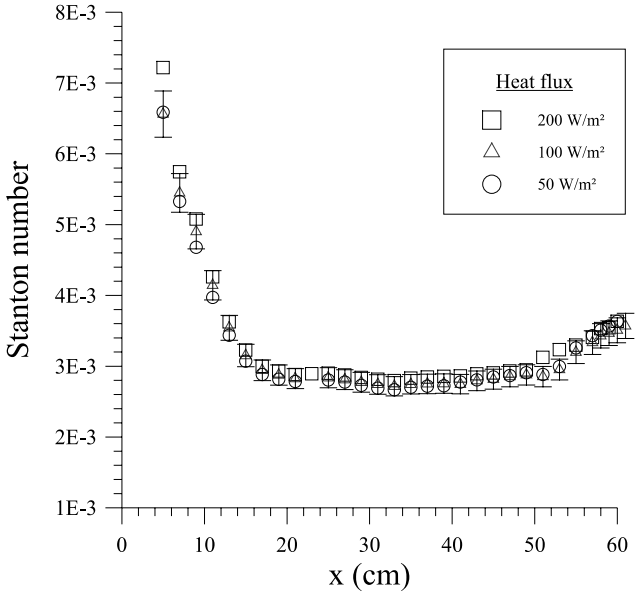

Fig. 4. Effect of wall heat flux on longitudinal Stanton number.

results difficult. Kamotani et al. (1985) have shown that this effect depends on the ratio Gr/G^2 and becomes non-negligible when this ratio exceeds unity. In the present case this ratio is much smaller than the unity ($Gr/G^2 = 0.093$), which ensures that the destabilizing effect due to the heating is negligible compared to the Görtler instability effect. Fig. 4 confirms this conclusion by showing that different values of wall heat flux do not change the longitudinal evolution of the convective heat transfer coefficient. Multiplying the wall heat flux by 4 makes the change in Stanton number remain below the measurement uncertainty (5%). Therefore we use the velocity field measurements in the isothermal conditions to interpret the temperature field and heat transfer results.

3.2. Perturbation amplification by Görtler instability

Experiments were run at nominal freestream velocity of $U_n = 4.8$ m/s and wall heat flux of $\varphi_w = 200$ W/m^2. The forced wavelength was 3 cm. Velocity and temperature fields were measured in the y–z planes at the following distances x from the leading edge: $x = 15$, 25, 31, 35, and 49 cm. At each station velocity and temperature were scanned in the y–z plane starting from the wall up to the boundary layer edge. Each data set consisted of 900 measurement points, 60 points at each given y distance from the wall. The distance between two neighboring points in the z direction was 1 mm. In this manner velocity and temperature distributions across the boundary layer at each station were obtained. Fig. 5 shows the isocontourlines of dimensionless velocity U/U_p at several positions from the leading edge, where U_p is defined as $U_p(y) = U_{pw}/(1 - y/R)$, U_{pw} being the potential wall velocity and R the radius of curvature of the concave wall ($R > 0$ for the concave wall). This choice of velocity normalization readily allows comparison of the nondimensional velocity and temperature profiles. Fig. 6 shows the isocontour lines of the nondimensional temperature $(T_w - T)/(T_w - T_\infty)$. Wall temperatures were obtained by the wall thermocouples.

Figs. 5 and 6, very similar, show the effects of amplification of initial perturbations by Görtler instability. At $x = 31$ cm, four maxima located at $z = 0.5$ cm, $z = 1.4$ cm, $z = 4.2$ cm and $z = 5$ cm are discernible in Fig. 5. They represent the upwash regions of the Görtler vortices. In the same figure one can also observe the minima at $z \approx 0.2$ cm, $z \approx 0.9$ m, $z \approx 1.8$ cm, $z \approx 3.9$ cm, $z \approx 4.6$ cm and $z \approx 5.4$ cm. These are the downwash zones, which are more or less extended. Due to the closeness of the two pairs of vortices, the downwash region between them shrinks while the vortex intensity is increased. On the other hand, the upwash zones situated on the two sides of the double vortex pairs are extended and therefore their effect is diminished. These measurements show longitudinal evolution of the double vortex pairs and particularly the independence of the spatial structure of the neighboring vortices and their breakdown into turbulence.

The above observations confirm that four pairs of Görtler vortices are present, two pairs symmetrically located on either side of position $z = 1$ cm and the other two on either side of position $z = 4.7$ cm. These two positions are very close to the spanwise positions of the wavelength forcing wires, $z = 1$ and 4 cm. Previous experiments (Ajakh et al., 1999) have thoroughly documented the existence of two pairs (instead of one pair) of Görtler vortices behind each perturbation wire.

Fig. 6 shows the temperature signature of Görtler vortices. The maxima observed in this figure represent the upwash regions where hot fluid particles close to the wall are deflected away from it by the action of Görtler vortices. The fact that the temperature isocontour lines follow very closely the isocontour lines of velocity confirms that the effect of the thermal field on the velocity field is negligible, as intended in designing the test section; temperature is a passive tracer. Similar observations have been made by Liu and Lee (1995).

The detailed velocity and temperature field measurements at different axial positions show that the amplification of perturbations by Görtler vortices tends progressively to distort the spanwise velocity and temperature profiles. A criterion based on the spanwise distortion of velocity and temperature profile is defined to quantify the amplification of perturbations. Ajakh (1997) and Ajakh et al. (1996) defined an amplification parameter P_z, based on the spanwise gradient of the streamwise velocity, $\partial U/\partial z$

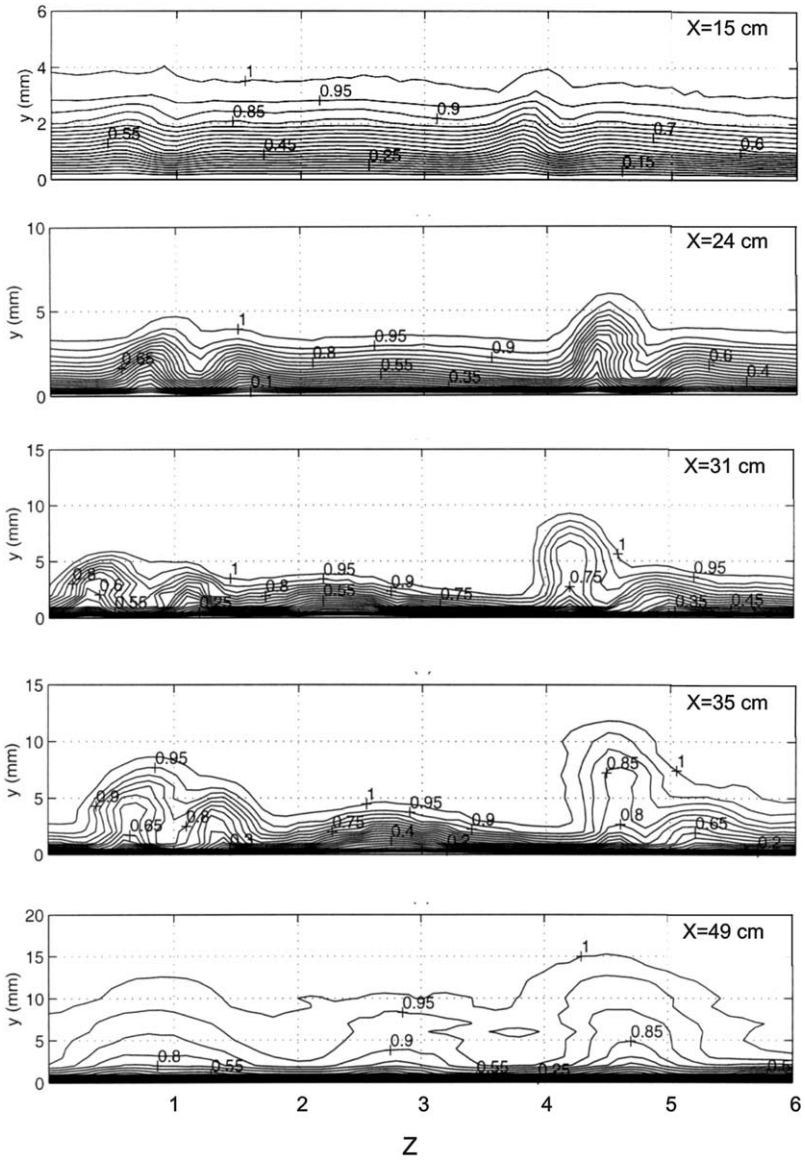

Fig. 5. Streamwise evolution of isocontours of $U_{(z)}/U_{(p)}$ (%) for $U_n = 4.8$ m/s, $\lambda = 3$ cm, $\varphi_p = 200$ w/m^2.

$$P_z = \int_{y=0}^{\infty} \int_{z=0}^{2\lambda} \left| \frac{\partial U}{\partial z} \right| \mathrm{d}x\,\mathrm{d}y.$$

Perturbation amplification and Görtler vortex growth distort both wall-normal and spanwise velocity and temperature profiles. However, it is found that this growth and the eventual appearance of the secondary instability in the vortices are much better correlated with the spanwise distortion of the axial velocity profiles.

The isocontour lines of temperature and velocity reported above showed a close similarity between the velocity and temperature fields. Therefore we have defined a parameter based on the spanwise distortion of the temperature profiles, $\partial T/\partial z$, in order to quantify the growth of the Görtler vortices by their temperature signature. This parameter P_{zT} is defined as

$$P_{zT} = \int_{y=0}^{\infty} \int_{z=0}^{2\lambda} \left| \frac{\partial T}{\partial z} \right| \mathrm{d}z\,\mathrm{d}y.$$

Fig. 7, showing the evolution of P_z and P_{zT} in the streamwise direction, reveals an exponential amplification of the perturbation with x of the form $Ae^{\beta x}$, where β is the amplification rate of the perturbations. Both parameters P_z and P_{zT} show a monotonic increase with x up to axial position $x = 31$ cm. In this zone the Görtler vortices are amplified and consequently distort the velocity and temperature profiles. After $x = 31$ cm the amplification parameters decrease with x, implying that the difference between velocity profiles in downwash and upwash regions is becoming less and less significant. This is the result of the destruction of the organized vortex motion and homogenization of the velocity and

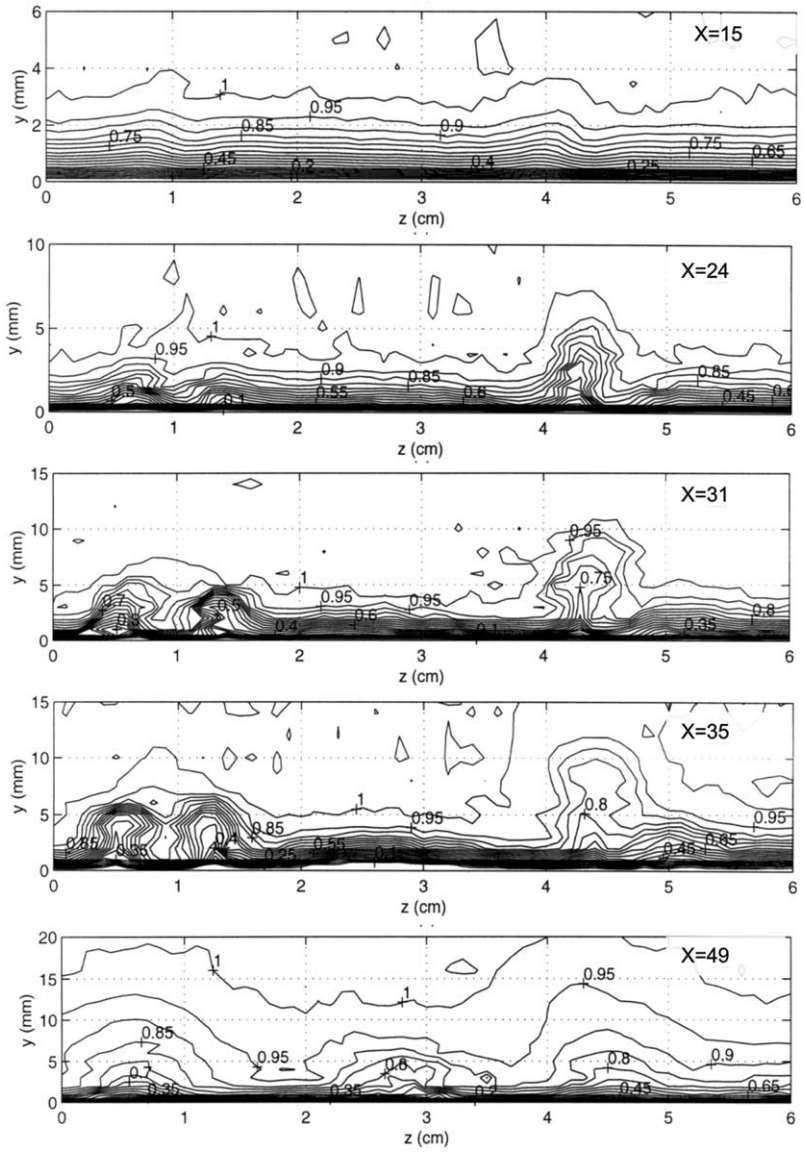

Fig. 6. Streamwise evolution of isocontours of $(T_w - T_{(z)})/(T_w - T_\infty)$ (%) for $U_n = 4.8$ m/s, $\lambda = 3$ cm, $\varphi_p = 200$ w/m^2.

temperature field under the effect of the transition to turbulence. It should be recalled that, in the zone of vortex amplification, the amplification rate β calculated from P_z and P_{zT} is close to $\beta \approx 0.06$. This confirms that the evolution of streamwise vortices can equally be determined by thermal or hydrodynamic measurements, and that temperature acts as a passive tracer in this evolution.

3.3. Longitudinal evolution of the Stanton number

Vortical motion of Görtler vortices has a direct effect on heat transfer from the concave wall to the boundary layer. Therefore, it is plausible to expect that vortex growth and transition to turbulence influence the wall heat transfer. It is the aim of this section to examine this influence.

Wall heat transfer is identified by the Stanton number $(St = \varphi_w/(\rho C_p U_n \Delta T) = h/(\rho C_p U_n))$, which is calculated from the measurement of the wall and boundary layer temperatures.

The vortex-triggering grid in front of the model leading edge was designed and positioned in such a way that the thermocouples imbedded in the model surface in the axial direction detect two upwash zones at $z = 4$ and $z = 7$ cm as well as a downwash zone at $z = 5.5$ cm. However, as explained in the previous section, two pairs of vortices (instead of one pair) were generated behind each vortex-triggering wire. Therefore it was very difficult to match the upwash and downwash regions of these vortices with the pre-determined positions of the thermocouple lines; the wires fixed the wavelength between a double pair of vortices but not their natural wavelength. Precautions were taken to refine the ther-

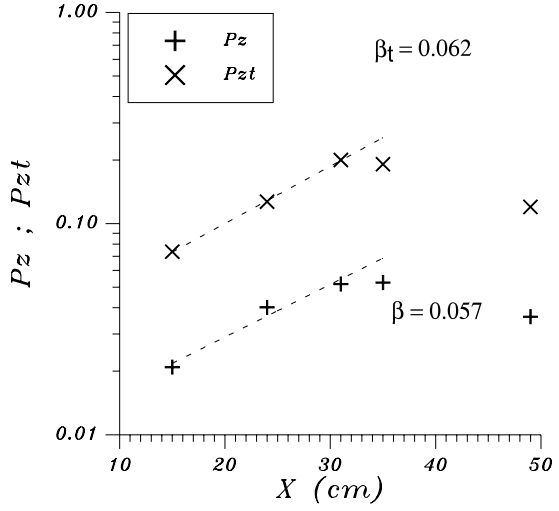

Fig. 7. Spatial amplification of perturbations. Comparison between the amplification coefficient calculated with the velocity gradient and with temperature gradient.

mocouple positions by adding spanwise rows of thermocouples at $x = 5$, 15, 31, 49, and 58 cm in which the thermocouples were spaced every 5 mm. However, since the distance between two adjacent thermocouples is large compared with the dimensions of downwash regions, the thermocouples measure only average wall temperature, whose evolution we follow in the streamwise direction.

Fig. 8 shows the evolution of the Stanton number versus x for nominal velocity $U_n = 4.8$ m/s. The Stanton number follows the laminar flat-plate curve up to $x = 15$ cm, corresponding to $Re_x \approx 4.04 \times 10^4$ ($G_\theta \approx 3.8$). In this region the effect of Görtler vortices is too weak to influence heat transfer from the wall. From $x = 15$ to $x = 31$ cm ($Re_x = 4.57 \times 10^4$ ($G_\theta \approx 4.2$) to $Re_x = 8.34 \times 10^4$ ($G_\theta \approx 6.6$)), the Stanton number deviates from the laminar flat plate and achieves a plateau with $St = 0.0027$. The appearance of this plateau coincides with the amplification zone of the Görtler vortices, as seen in Fig. 7, and corresponds to the effect of longitudinal vortices in increasing the wall heat transfer. After $x = 33$ cm (corresponding to $Re_x = 1.1 \times 10^5$ ($G_\theta \approx 6.9$)), one observes a net increase of Stanton number with x. This phenomenon starts from the point where the perturbation growth is saturated and the perturbation amplification rate shows the transition to turbulence. From $x = 41$ cm ($Re_x = 1.7 \times 10^5$ ($G_\theta \approx 8.1$)), the Stanton number increase begins to relax towards a curve parallel to that of turbulent boundary layer over a flat plate.

The effect of free stream velocity on the Stanton number is shown in Fig. 9 for nominal velocities between 2 and 9 m/s. In this figure, the evolution of the Stanton number versus Reynolds number is represented. Correlations for a laminar and turbulent boundary layer on flat wall are also superposed.

Below 5 m/s, the curves follow the same tendency as described in the previous section. At low Reynolds numbers, they follow the laminar flat plate curve. They deviate from it at $Re_x = 6.01 \times 10^4$ for $U_n = 4.8$ m/s, $Re_x = 4.2 \times 10^4$ for $U_n = 3$ m/s and $Re_x = 3.3 \times 10^4$ for $U_n = 2$ m/s, and a constant Stanton number plateau begins to develop (Toé, 1999), representing heat transfer enhancement by Görtler vortices. For $U_n = 2$ m/s at $Re_x = 6.6 \times 10^4$ ($x = 51$ cm), the Stanton number is 50% higher than that for a flat plate at the same Reynolds number. For $U_n = 3$ m/s at $Re_x = 8 \times 10^4$ ($x = 41$ cm) it is 43% higher, and it is 19% higher for $U_n = 4.8$ m/s at

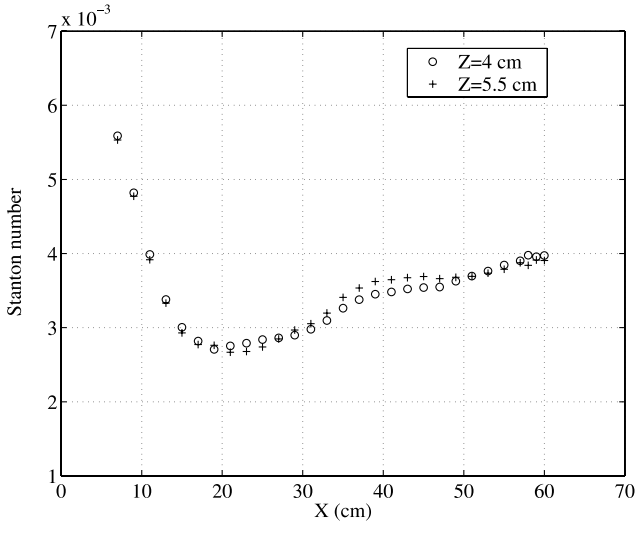

Fig. 8. Streamwise evolution of Stanton number at spanwise positions $z = 4$ cm and $z = 5.5$ cm for $U_n = 4.8$ m/s, $\lambda = 3$ cm, $\varphi_p = 200$ w/m^2.

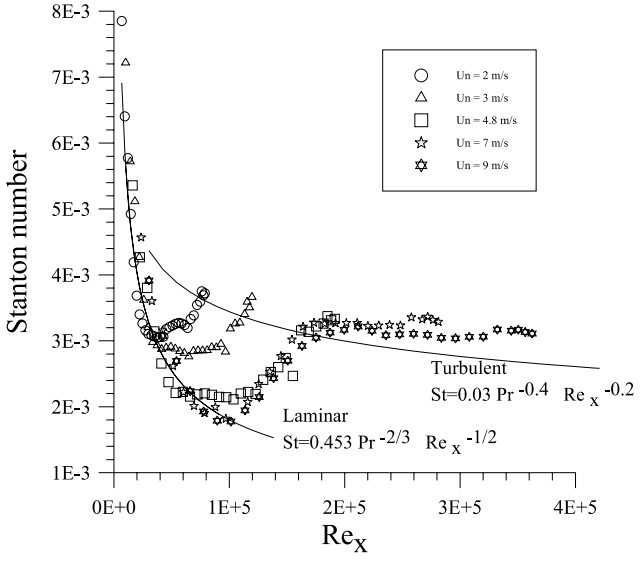

Fig. 9. Evolution of the Stanton number versus Reynolds number for various free stream velocities.

$Re_x \approx 10^5$ ($x = 33$ cm). The plateau can be interpreted as an equilibrium between the boundary-layer thickening effect (reduction in Stanton number) and the mixing effect of the Görtler vortices (increase in Stanton number). The end of the plateau corresponds to the state in which the vortices start to become time-dependent. The Stanton number increases under the joint effect of axial vorticity and vortex meandering until it reaches the turbulent boundary layer curve, where the vortex structure has broken down and turbulence has set in. Beyond this point the experimental points follow the trend of the turbulent flat plate curve.

If the model wall surface were longer, one would expect the curve of Stanton number to relax towards that of turbulent flat plate boundary layer. The maximum augmentation (compared to the laminar flat plate boundary layer) of Stanton number occurs at the three lowest nominal velocities, at the end of the characteristic plateau where the vortices are fully developed. We noted before that the increase in the convective heat transfer coefficient beyond the end of the plateau is due to the temporal fluctuation of the vortices, marked by saturation of the amplification criterion.

For nominal velocities of 7 and 9 m/s, the transition scenario is different. Fig. 9 shows that the plateau of constant Stanton number does not appear. Experimental points follow the laminar flat plate curve up to $Re_x = 10^5$, then deviate from it and rapidly increase to join the turbulent flat plate curve. Transition from the laminar flat plate curve ($Re_x = 10^5$) appears at $x = 16$ cm for $U_n = 9$ m/s and at $x = 19$ cm for $U_n = 7$ m/s. Since the curved part of the model starts at $x = 9$ cm, the above distances are too small to let the Görtler vortices develop before a flat-plate-type transition eliminates their effect. Though the detailed transition mechanism for $U_n = 9$ m/s and $U_n = 7$ m/s was not studied here, this fast transition suggests that bypass transition occurs here. One notices, however, that for the last two nominal velocities, once the flow has become fully turbulent, it follows the trend of the curve for a turbulent flat plate boundary layer with a slightly higher value of the Stanton number.

The behavior of the Stanton number shown in Fig. 9, in which one can distinguish laminar transitional and turbulent zones, has not been reported before. In an analogous situation, namely a heated flat-plate boundary layer rotating around an axis parallel to its leading edge, Yamawaki et al. (2001) observed similar Stanton number behavior. If the Coriolis force is normal and toward the solid wall, regular longitudinal vortices similar to Görtler vortices appear that analogously contribute to heat transfer enhancement. The flat plate in Yamawaki et al.'s experiment was not long enough to allow transition to a fully turbulent boundary layer, or to allow comparison with a stationary turbulent flat plate. Nevertheless, when the rotating boundary layer became turbulent, a slight increase of Stanton number over that of a stationary flat plate turbulent boundary layer was observed. This observation is also in agreement with the result shown in Fig. 9.

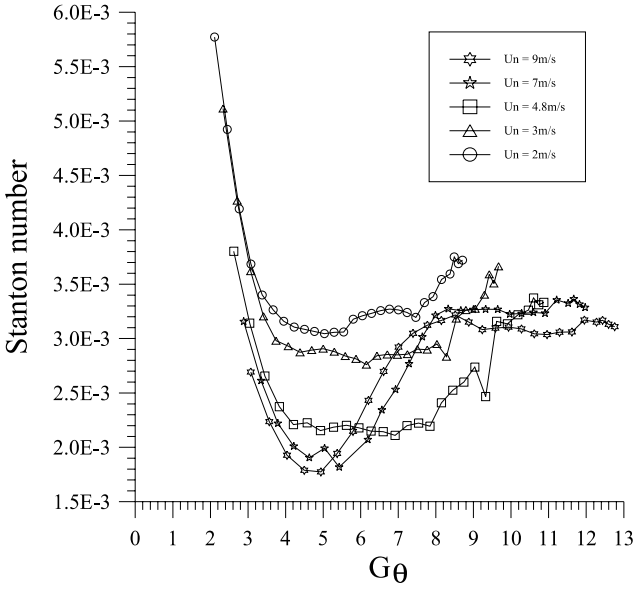

Fig. 10. Evolution of the Stanton number versus Görtler number for various free stream velocities.

Representing the Stanton number as a function of Reynolds number facilitates comparison of the behaviour of a concave boundary layer with a flat one. However, it masks the effect of the Görtler number, which is the real control parameter, especially for those cases where the regime remains laminar with vortices superposed on it. Therefore we show in Fig. 10 the evolution of Stanton number versus Görtler number. In this representation, one can notice that the general shapes of the curves for nominal velocities below 5 m/s are identical; the end of the characteristic plateau coincides with Görtler number between 7 and 8. Liepmann (1945) in his preliminary experiments on a concave wall found that the transition to turbulence occurs at G_θ between 6 and 9. Crane and Sabzvari (1989) have shown experimentally that the increase of Stanton number on a concave wall with respect to a flat plate becomes observable beyond $G_\theta \approx 10$. This presentation, however, did not let the curves of Stanton number versus Görtler number collapse for different nominal velocities. The results also confirm that in the present experimental setup for nominal velocities higher than 7 m/s Görtler vortices do not have enough resident time on the concave wall to develop and show their effect on heat transfer. Transition occurs very early on the concave wall and therefore the characteristic plateau is extremely short.

4. Conclusions

An experimental apparatus was specifically designed to investigate the effect of Görtler instability on the heat transfer from a concave wall. To fix the position of the vortices they were triggered by a grid located in front of the test section. Velocity and temperature fields in the boundary layer were measured and isocontour lines of each were plotted at five axial positions on the test section. These isocontour lines showed that two pairs of Görtler vortices were generated behind each triggering wire, one pair on each side of it. This result, while contrary to what was commonly expected, is in agreement with the previous results of Ajakh et al. (1999) obtained on a similar model.

Velocity and temperature isocontour lines are found to be very similar; a one-to-one relation was found between the upwash regions and hot spots, on the one hand, and the downwash regions and cold points on the other (in the hydrodynamic and thermal boundary layers respectively).

Görtler vortices appear because of the amplification by the centrifugal instability mechanism of the perturbations entering the boundary layer, and hence the amplification rate of the perturbations is of prime interest. In this work a new criterion P_z is suggested based on the spanwise gradient of the streamwise velocity $\partial U/\partial z$. The advantage of this criterion over those previously proposed based on the integral of the perturbation component of the streamwise velocity is that in the former the modification of the base flow by instability is automatically taken care of. A similar criterion but based on the spanwise gradient of the temperature P_{zT} is also proposed here. Both criteria can be used to estimate the amplification of perturbations by Görtler instability. The value of the exponential amplification factor is around 0.06.

The perturbation amplification criterion P_z (or $P_{z\mathrm{T}}$) reaches a maximum value at $G_\theta \approx 6.6$ ($x = 31$ cm), which corresponds to the maximum amplification of the Görtler vortices. Beyond this point P_z (or $P_{z\mathrm{T}}$) decreases with G_θ showing the disappearance of distinct upwash and downwash zones in the boundary layer andindicating the end of time-independent organized vortex structures.

The effect of Görtler vortices generated by the instability mechanism on the wall heat transfer is also investigated by following the evolution of the Stanton number along the concave wall and with freestream velocity. Three distinct zones are discernible:

- A first zone close to the leading edge where the flow is laminar and the Görtler vortices are still weak. In this zone the value of the Stanton number is equal to that in a laminar flat-plate boundary layer.
- A second zone follows the first where the boundary layer is unstable; it is a laminar boundary layer over which the Görtler vortices are superposed. In this zone the Stanton number is constant; it does not vary with the Görtler number. The end of this zone coincides with the axial position where the value of P_z (or $P_{z\mathrm{T}}$) corresponds to a Görtler number between 6 and 7. Therefore, the vortex amplification results are confirmed by the Stanton number measurements.
- Finally, beyond the end of this region the Görtler vortices become unstable and eventually break down in turbulence. In this transition zone the Stanton number increase rapidly and reaches values slightly higher than those of a turbulent boundary layer over a flat plate. This scenario occurs for moderate freestream velocities ($U_\mathrm{n} < 5$ m/s). At higher speeds the transition from laminar to turbulent regime is direct and does not pass through the constant Stanton number regime.

5. Discussion

Turbulent boundary layers over a concave wall may show distinct regular streamwise vortices if the vortices were generated in a laminar concave boundary layer prior to entering the turbulent boundary layer. Otherwise, when a well-developed turbulent boundary layer encounters a concave wall, weak, irregular and highly intermittent streamwise vortices may appear. In the latter case, the spanwise variation of flow parameters such as δ, C_f, Nu and the velocity profile is modest. Most heat-transfer experiments in turbulent boundary layers have been carried out for this latter case.

Mayle et al. (1977) showed an increase of St in concave boundary layers over that of flat-plate boundary layers, and a decrease for the convex boundary layers. Martin and Brown (1979) found that at $Re = 8.8 \times 10^5$, the local heat transfer exceeds that of the flat plate by a factor of 2 and is insensitive to turbulence intensity for Tu ranging from 6.6% to 9.1%. Experiments of Simonich and Moffat (1984) showed a 20% heat-transfer enhancement resulting from the augmentation of mixing due to curvature, but no stationary vortex structure was observed. Due to the intermittency (in both time and space) of the streamwise vortices in the turbulent boundary layers, it is difficult to perform systematic experiments to assess the heat-transfer enhancement resulting from the concave curvature. In addition, the theory of centrifugal instability in turbulent boundary layers is not sufficiently developed to formulate the experimental observations properly.

When the turbulent boundary layer is uniform and two-dimensional in mean, longitudinal vortices are generated by the interaction between the finite intensity

perturbations caused by the largest eddies and the centrifugal instability. The most energetic eddies are amplified and will evolve into longitudinal vortices as they convect downstream. Since such eddies are randomly distributed at the onset of curvature, no steady vortex pattern will emerge (Barlow and Johnson (1985)).

In the present study turbulence is emerged from the successive transitions of Görtler vortices triggered in a laminar boundary layer by external forcing. Therefore, the origin of turbulence is different from the above mentioned case. Experimental observations of Peerhossaini and Wesfreid (1988b) by using Laser-Induced Fluorescence (LIF) visualization technique in a water tunnel showed that at G_θ higer than 7 the Görtler vortex flow becomes turbulent. The Görtler vortices, though distorted keep their general shape and appear intermittently in the original spanwise position of their initial appearance. They look like very large coherent structures superimposed on the boundary layer, which would have not existed in a turbulent boundary layer over a flat plate. These enhanced mixing and explain the extra heat transfer exhibited by the concave turbulent boundary layer compared with the boundary layer on a flat plate. The authors compared the video images of their visualization with those of Barlow and Johnson (1985) and found a striking resemblance between them: in both cases the large coherent structures appeared intermittenly in time and space at distinct upwash regions.

References

Ajakh, A., Kestoras, M.D., Toé, R., Peerhossaini, H., 1999. Influence of forced perturbations in the stagnation region on Görtler instability. AIAA J. 37, 9.

Ajakh, A., 1997. Etude expérimentale de l'instabilité de Görtler: identification de critères d'amplification et de l'inremittence; effet de bord d'attaque et forçage de longueur d'onde. Ph.D. Thesis, University of Nantes.

Ajakh, A., Toé, R., Kestoras, M.D., Peerhossaini, H., 1996. Experiments on the Görtler instability: its relation to transition to turbulence, ASME Fluids Engineering, FED, 237, 613–621.

Barlow, R., Johnson, J.P., 1985. Roll-cell structure in a concave turbulent boundary layer. In: AIAA 23rd Aerospace Science meeting, Reno, AIAA Paper 85-0297.

Blackwell, B.F., Moffat, R.J., 1975. Design and construction of a low-velocity boundary-layer temperature probe. J. Heat Transfer, Trans. ASME, 97, 313–315.

Crane, R.I., Sabzvari, J., 1989. Heat transfer visualization and measurement in unstable concave-wall laminar boundary layers. ASME J. Turbomach. 111, 51–56.

Crane, R.I., Umur, H., 1990. Concave wall laminar heat transfer and Görtler vortex structure: effects of pre-curvature boundary layer and favourable pressure gradients. In: Gas Turbine and Aeroengine Congress, Bruxelles, June 11–14, ASME Paper No. 90-GT-94.

Floryan, J.M., Saric, W.S., 1982. Stability of Görtler vorices in boundary layers. AIAA J. 20 (3), 316–324.

Görtler, H., 1940. Über eine dreidimensionale Instabilität laminarer grenzschichten an konkaven Wänden. Math. Phys. Klasse, 2, 1–16. Translated by Görtler H. On the three-dimensional instability of laminar boundary layers on concave walls. Technical report, NACA, 1954, TM-1375.

Guo, Y., Finlay, W.H., 1994. Wavenumber selection and irregularity of spatially developing nonlinear Dean and Görtler vortices. J. Fluid Mech. 264, 1–40.

Kamotani, Y., Lin, J.K., Ostrach, S., 1985. Effect of destabilizing heating on Görtler vortices. J. Heat Transfer 107, 877–882.

Kottke, V., 1988. On the instability of laminar boundary layer along a concave wall towards Görtler vortices. In: Propagation and Non Equilibrium Systems. Springer, Berlin.

Liepmann, H.W., 1945. Investigation of boundary layer transition on concave wall. Technical report, NACA.

Liu, J.T.C., Lee, K., 1995. Heat transfer in a strongly nonlinear spatially developing longitudinal vorticity system. Phys. Fluids 7, 559–599.

Martin, B.W., Brown, A., 1979. Factors influencing heat transfer to the pressure surfaces of gas turbine blades. Int. J. Heat and Fluid Flow 1, 107–119.

Mayle, R.E., Kopper, F.C., Blair, M.F., Bailey, D.A., 1977. Effect of streamline curvature on film cooling. ASME J. Engineering for Power 99, 77–82.

McCormack, P.D., Welker, H., Kelleher, M., 1970. Taylor–Görtler vortices and their effect on heat transfer. ASME J. Heat Transfer 92, 101–112.

Peerhossaini, H., Wesfreid, J.E., 1988a. Les tourbillons de Görtler et leurs influence sur les turbines à gaz. Bull. Assoc. Tech. Maritime Aéronaut. 88, 361–381.

Peerhossaini, H., Wesfreid, J.E., 1988b. On the inner structure of Görtler vortices. Int. J. Heat Fluid Flow 9, 12–18.

Peerhossaini, H., Wesfreid, J.E., 1988c. Experimental study of the Taylor–Görtler instability. In: Brand, H., Boccara, N. (Eds.), Propagation in Systems Far from Equilibrium. Springer, Berlin, pp. 399–412.

Peerhossaini, H., Bippes, H., Steinbach, D., 1990. A model for the experimental study of curvature effects on transition. La Recheche. Aérospatiale 6, 15–21.

Peerhossaini, H., 1997. On the effects of streamwise vortices on wall heat transfer. In: Shah, R. (Ed.), Compact Heat Exchangers for Process Industries. Begell House Publishers, New York, pp. 571–589.

Peerhossaini, H., Bahri, F., 1998. On the spectral distribution of the modes in nonlinear Görtler instability. Exp. Thermal Fluid Sci. 16, 195–208.

Simonich, J.C., Moffat, R.J., 1984. Liquid crystal visualization of surface heat transfer on a concavely curved turbulent boundary layer. ASME J. Engineering for Gas Turbine and Power 106, 619–627.

Smith, S.T., Haj-Hariri, H., 1993. Görtler vortices and heat transfer. A weakly nonlinear analysis. Phys. Fluids A 5, 2815–2825.

Swearingen, J.D., Blackwelder, R.F., 1985. The growth and breakdown of streamwise vortices in the presence of a wall. J. Fluid Mech. 182, 255–290.

Toé, R., 1999. Etude expérimentale de l'instabilité de Görtler: Instabilité secondaire et effets des tourbillons de Görtler sur les phénomènes de transfert thermique. Ph.D. Thesis, University of Nantes.

Yamawaki, D., Obi, S., Masuda, S., 2001. Heat transfer in transitional and turbulent boundary layer with system rotation. In: Turbulent Heat Transfer III, Anchorage, Alaska, March 19–21, 2001.